Design of a High-Gain Millimeter Wave Array MIMO Antenna for 5G

Wenhui Liu[1] and Xinchun Li[2, *]

[1]*School of Electronics and Information Engineering, Liaoning Technical University, Huludao 125105, China*
[2]*Liaoning Institute of Science and Engineering, Jinzhou, China*

ABSTRACT: To deal with the problems of low gain and low data transmission rate of millimeter wave antenna during long-distance transmission, a high-gain millimeter wave array multiple-input-multiple-output (MIMO) antenna with series-parallel hybrid feed is proposed. The radiating structure consists of a combination of multiple rectangular patches, to make the proposed design resonate within the desired frequency band of 39 GHz. The antenna line array consists of eight radiating patches connected in series via transmission lines, providing an operating bandwidth of 1.02 GHz and a peak gain of 15.9 dB, and utilizing the Chebyshev synthesis method to control the side lobe level below -20 dB. In order to obtain higher gain, two antenna line arrays are connected through a Y-shaped feeding network, which utilizes the mutual coupling between the antennas to increase the bandwidth of the antenna to 1.25 GHz and provide a simulated gain of 17.6 dBi. Furthermore, the proposed array antennas are placed side-by-side to form a four-port MIMO antenna, which does not require any decoupling structure and has the isolation of more than 25 dB. The radiation efficiency is as high as 99%, the Envelope Correlation Coefficient (ECC) less than 0.003, and the Diversity Gain (DG) greater than 9.98. The measured results show that the operating frequency band of the antenna is $38.0 \sim 39.6$ GHz, and the operating bandwidth is 1.6 GHz. In the operating frequency band, the peak gain of the antenna is 17.45 dBi. Finally, the frequency characteristics and radiation characteristics of the antenna when bending are analyzed. The results show that the bending of the antenna leads to a slight shift in the resonant frequency, but the relative bandwidth remains unchanged. The gain has decreased, indicating that the antenna is able to work normally after bending and has a wider range of application scenarios.

1. INTRODUCTION

With the rapid development of wireless communication technology, the existing spectrum resources are insufficient to meet the growing demand. In 2019, 3rd Generation Partnership Project (3GPP) divided the millimeter wave frequency band of $24.25 \sim 52.6$ GHz (i.e., FR2 frequency band) for 5th generation mobile networks (5G) communication [1]. Among them, the relatively low additional attenuation during the transmission of 39 GHz millimeter waves offers a significant advantage, leading to its widespread application in millimeter wave communication systems. Millimeter wave wireless communication, with its remarkable characteristics such as high data rate, ultra-low latency, and high spectrum reusability [2], has opened up new possibilities for cutting-edge technology applications such as autonomous driving, telemedicine services [3], and virtual reality [4, 5]. In millimeter-wave communication systems, the research of millimeter-wave antennas has also received extensive attention from academia and industry [6, 7]. The millimeter-wave array multiple-input multiple-output (MIMO) antenna combines MIMO technology with array technology, enabling the antenna to harness the diversity characteristics of MIMO to enhance communication rates and channel capacity, while also utilizing array synthesis techniques to design high gain and low side lobe antennas that increase the transmission distance of millimeter-wave signals and

reduce interference with signal transmission caused by clutter [8]. MIMO array antennas offer significant advantages in millimeter wave communication systems by effectively reducing signal transmission costs, maximizing the utilization of limited resources to improve signal coverage, and enhancing the reliability and stability of communication systems. They meet the ever-growing demands for communication channel capacity and communication quality [9–11]. However, the main problem facing the design of MIMO antenna is how to suppress the crosstalk caused by the mutual coupling between antenna elements in a limited space. In order to reduce the coupling between antennas, scholars have done a large number of related researches. At present, the common methods to reduce the coupling between antennas are etching defective ground structure, diversity technology, floor branch or parasitic structure, neutralization line technology, electromagnetic band-gap, and adding decoupling network [12–16]. However, these decoupling methods not only have certain limitations on the antenna gain, efficiency, and application scenarios, but also increase the antenna size and the design difficulty of the feed, so how to reduce the inter-antenna coupling and improve the antenna isolation and gain has been generally emphasized. Ref. [17] proposes a MIMO antenna for 5G which improves antenna isolation by adding a ground decoupling structure; however, the antenna gain is only 6.5 dBi, and the ECC is less than 0.18. Ref. [18] proposes a coplanar waveguide (CPW) fed 2-

* Corresponding author: Xinchun Li (550128966@qq.com).

port MIMO structure with common ground, and a aperture-coupled patch configuration fed by a CPW transmission line is adopted to design an elementary antenna. The antenna isolation is greater than 25 dB using orthogonal distribution, but the antenna gain is only 8 dBi, and due to the adoption of a double-layer board structure for the antenna, the manufacturing process of the antenna becomes relatively complex, requiring higher precision in craftsmanship and increased costs. In [19], a slotted design is used to make the isolation of the MIMO antenna greater than 17 dB with the gain of 8.3 dBi. Ref. [20] also proposes a defected ground structure (DGS) based MIMO antenna for 5G applications, where the isolation is greater than 29 dB, and the gain is 6.1 dBi. Ref. [21] proposes a metasurface MIMO array antenna. Through the metasurface array structure composed of CSR, the isolation between MIMO antenna elements is greater than 45 dB; the gain of the antenna reaches 10.27 dBi; ECC is lower than 0.0008; and the DG is greater than 9.98. Ref. [22] proposes a two-port MIMO array antenna for 5G applications. The isolation between antenna ports exceeds 28.0 dB; the radiation efficiency is greater than 93%; the maximum gain is 15.46 dBi; and the ECC is lower than 0.0001. Ref. [23] proposes an array MIMO antenna for 5G communication system. The array antennas are placed orthogonally to form an array MIMO antenna. The resonant frequency of the antenna is 37 GHz; the isolation is greater than 40 dB; the maximum gain is 12.8 dBi; the radiation efficiency is more than 85%; ECC is less than 0.00014; and DG is close to 10. Ref. [24] proposes a millimeter wave array MIMO antenna with isolation greater than 30 dB, using four antenna elements in an antenna array, connected with a T-shaped feeding network, and provides a 12.5 dBi peak gain and radiation efficiency of 91.5%.

In summary, different techniques have been used in these designs to mitigate the coupling currents between the antenna elements, but either the complexity of the design is increased, or low gain is obtained, or some of them have low isolation; however, both factors (isolation and gain) are important for the antenna to work efficiently. Thus, considering the limitations of the above antenna design, in this work, we aimed to design a four-port array MIMO antenna supported by full ground plane for 5G applications.

The following are the key contributions of the proposed work:

1. The Chebyshev synthesis method is applied to design the tapered antenna line array to reduce the side lobe level of the antenna.

2. Design the shaped power to connect antenna arrays in parallel. The method of mixed series-parallel feeding is applied to increase the antenna gain to meet the requirements of long-distance communication, and the maximum antenna gain reaches 17.45 dBi.

3. The overall structure of planar array antenna does not involve geometric complexities. Our aim is to achieve high integration of array antenna and MIMO configuration while keeping the antenna element structure design as simple as possible to avoid design complexities and fabrication challenges. The four-port array MIMO antenna with high isolation without adding a decoupling structure is designed to solve the prob-

lem of low data transmission rates. Stable reflection coefficient S_{ii} response is generated from the array MIMO antenna at $f_0 = 39$ GHz. Low ECC value and high DG value are achieved which ensures a low correlation between the MIMO antennas.

4. The frequency characteristics and radiation characteristics of the array MIMO antenna under the condition of cylinder bending are tested and analyzed.

2. STRUCTURAL DESIGN OF ANTENNA UNIT

2.1. Infrastructure

The structure of the antenna element is shown in Fig. 1 and consists of a feeder line and a rectangular radiant patch. The length of the radiation patch is L_P, and the width is W_P. The dielectric substrate material is Rogers RT5880 with low loss ($\varepsilon_r = 2.2$, $\tan\delta = 0.0009$), and the thickness is 0.787 mm. The perimeter of the radiating patch is theoretically close to one dielectric wavelength. Considering the edge effect of the radiating patch, the dimensions of the rectangular patch antenna are calculated by the following formulas:

$$L_p = \frac{c}{2f\sqrt{\varepsilon_e}} - 2\Delta L \tag{1}$$

$$W_P = \frac{c}{2f}\left(\frac{\varepsilon_r + 1}{2}\right)^{-\frac{1}{2}} \tag{2}$$

$$\varepsilon_e = \frac{\varepsilon_r + 1}{2} + \frac{\varepsilon_r - 1}{2}\left(\sqrt{\frac{W_P}{12h + W_P}}\right) \tag{3}$$

$$\Delta L = 0.412 \frac{(\varepsilon_e + 0.3)(W_P/h + 0.264)}{(\varepsilon_e - 0.258)(W_P/h + 0.8)} \tag{4}$$
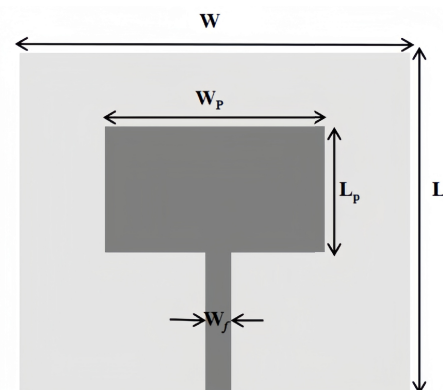
FIGURE 1. Antenna infrastructure.

In the formulas, L_P is the length of the radiation patch, W_P the width of the radiation patch, ε_e the effective dielectric constant of the dielectric substrate, ε_r the relative dielectric constant, h the thickness of the dielectric plate, ΔL the equivalent radiation slot width, and f the operating frequency of the antenna.
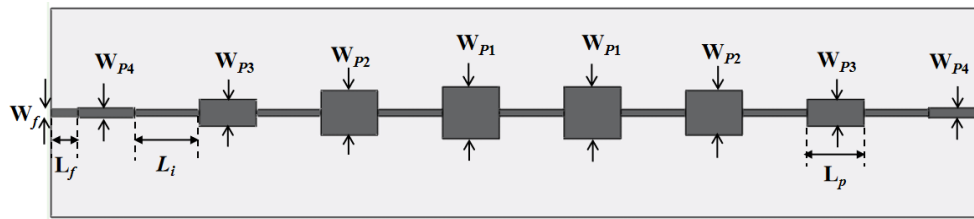
FIGURE 2. The structure of an eight-element series-fed linear array antenna.

2.2. Structural Design of Series-Fed Linear Antenna Array

An eight-element linear series-fed array antenna with symmetrical distribution of excitation amplitude and half wavelength spacing between array elements is designed by the Chebyshev synthesis method. In order to leave spare design space for actual simulation, the side lobe level of the antenna is preset to -25 dB, and the antenna gain is greater than 15 dBi. Firstly, it is necessary to calculate the distribution ratio of the excitation current amplitude of each array element.

According to the Chebyshev function form: $T_m(x) = \cos(mu)$, where $x = \cos(mu)$, by expanding it into the power polynomial of $\cos u$ to find the array factor polynomial of the array antenna.

Array factor of odd array antenna:

$$S_{odd}(u) = \sum_{N=1}^{M+1} I_n \cos[2(n-1)u] \tag{5}$$

Array factor of even-numbered array antenna:

$$S_{even}(u) = \sum_{N=1}^{M+1} I_n \cos 2(n-1)u \tag{6}$$

The antenna designed in this paper is an eight-element linear series-fed array antenna. Therefore, $N = 8$, $M = 4$, and the excitation current amplitude of each array element is determined by Equation (6), where d is the spacing of antenna elements, and λ is the free space wavelength. The calculation results show that $x_0 = 1.136$ and $R_0 = 17.78$. In practical engineering design, the normalized current amplitude distribution of each array element is calculated directly by using MATLAB to run the Chebyshev function as $I_4 : I_3 : I_2 : I_1 : I_1 : I_2 : I_3 : I_4 = 0.3778 : 0.5843 : 0.8424 : 1 : 1 : 0.8424 : 0.5843 : 0.3778$.

Eight array elements are connected in series to form a linear array, constituting the basic structure of the antenna, as shown in Fig. 2. Through the microstrip line to patch element connected in series, this feeding method is adjusted through the spacing of the patch element to change the phase of the excitation current, through the adjustment of the patch size to change the amplitude of the excitation current [25–27]. The spacing L_i of the antenna element L_i is $0.5\lambda_g$ [28]; the microstrip line width of the feed port is W_f; the length is L_f; the radiation patch width ratio needs to be based on the series-fed linear antenna array excitation amplitude distribution ratio after calculation; the width ratio of each antenna array element is

$W_{P1} : W_{P2} : W_{P3} : W_{P4} = 3.04 : 2.56 : 1.78 : 1.14$; the values of the width of each array element are $W_{P1} = 3.04$ mm, $W_{P2} = 2.56$ mm, $W_{P3} = 1.78$ mm, $W_{P4} = 1.14$ mm; and the widths of the antennas are $W_{P1} = 2.26$ mm, $W_{P2} = 1.938$ mm, $W_{P3} = 1.17$ mm, $W_{P4} = 0.42$ mm, respectively, which are obtained by the application of electromagnetic (EM) software CST Studio Suite (CST) to the antennas.

The S parameters of the antenna linear array are shown in Fig. 3. The resonant frequency of the antenna decreases with the increase of L_i. The resonant frequency of the black curve is 39 GHz, and the S_{11} value reaches -32.80 dB. At this time, $L_i = 2.839$ mm, with $S_{11} < -10$ dB as the standard definition, and the operating frequency band of the antenna is $38.48 \sim 39.50$ GHz.
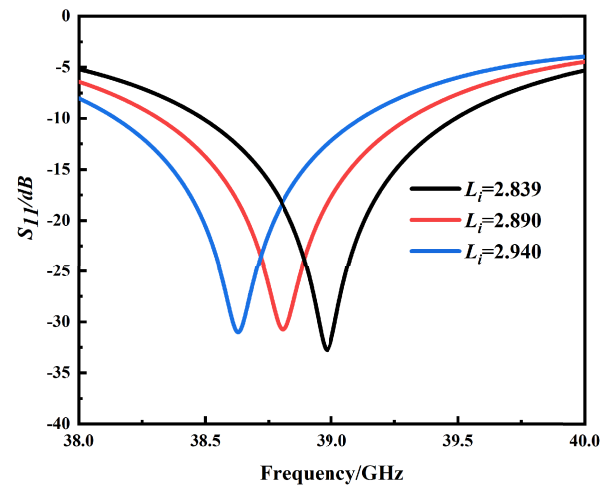
FIGURE 3. Antenna S_{11} parameters.

Figure 4 shows the radiation pattern of the optimized eight-array antenna. The data in the figure indicates that the peak gain of the antenna's E-plane is 15.9 dBi, and the side lobe level is -23.2 dB. The peak gain of the antenna's H-plane is 15.9 dBi, and the side lobe level is -21.3 dB.

3. DESIGN AND ANALYSIS OF SERIES-PARALLEL HYBRID-FED PLANAR ANTENNA ARRAYS

In order to obtain higher gain, it is necessary to increase the number of antenna elements [29]. In this section, a planar array antenna with 2×8 array elements is designed, and the spacing between the linear array antennas and the structure of the feed network are firstly defined. Since the designed antenna is a
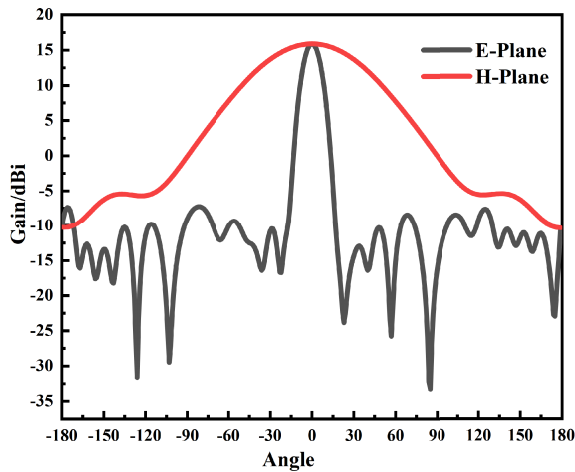
FIGURE 4. Radiation pattern.

side-shooting array, in order to prevent the appearance of grate lobes, the spacing between the linear array antennas is defined to be half a wavelength, which is further fine-tuned by combining the CST on the basis of comprehensively considering the mutual coupling between the arrays and the array size. The two linear arrays are formed into a high gain low side lobe array antenna without feed network. The optimal value of the spacing d is determined through simulation optimization to achieve the best impedance matching and radiation characteristics of the antenna, and the optimized spacing $d = 3.724$ mm.

3.1. Design of the Feeder Network

The feeding network of the array antenna consists of a Y-shape power divider, the use of which reduces the distance between the antenna patches and enhances the directivity of the antenna compared with the conventional T-shaped power divider. The power divider structure is shown in Fig. 5, which is designed from microstrip lines, where the different impedance transformations are ensured by tapered lines. The impedance of each channel is assumed to be 50 ohm. The two output ports are parallel with respect to the input port. Therefore, it is neces-

sary to transform the impedance of two outputs so that they have an equivalent impedance of 100 ohm at the node. Tapered lines provide additional degrees of freedom allowing impedance transformation over a wide bandwidth. The values of "W_f" and "W_{100}" are obtained by using the following equations:
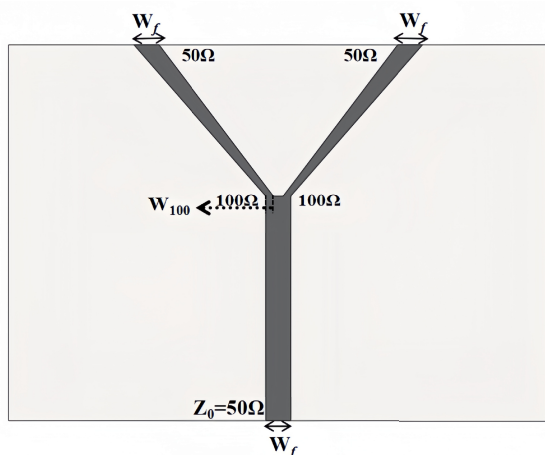
$$Z = 50\,\Omega = \frac{120\pi}{\sqrt{\varepsilon_e}\left[\frac{W_f}{h} + 1.393 + 0.667\ln\left(\frac{W_f}{h} + 1.444\right)\right]} \quad (7)$$

$$Z = 100\,\Omega = \frac{60}{\sqrt{\varepsilon_e}}\ln\left(\frac{8h}{W_{100}} + \frac{W_{100}}{4h}\right) \quad (8)$$

where the value of effective dielectric constant of the substrate ε_e in Equation (7) is the same value as that in Equation (3). The value of ε_e in Equation (8) ($W/h < 1$) is:

$$\varepsilon_e = \frac{\varepsilon_r + 1}{2} + \frac{\varepsilon_r - 1}{2}\left[\frac{1}{\sqrt{1 + 12\frac{h}{W}}} + 0.04\left(1 - \frac{w}{h}\right)^2\right] \quad (9)$$

3.2. Array Antenna Design

The planar array antenna structure is shown in Fig. 6, which contains 16 antenna elements, with 8 antenna elements in each line array, and each line array is fed in series. Two line arrays are fed in parallel through a Y-shaped power divider.

The S_{11} simulation diagram of the array antenna obtained after CST simulation optimization is shown in Fig. 7, which shows that the bandwidth of the antenna is from 38.38 GHz to 39.63 GHz; the return loss is 34 dB at the resonance frequency of 39 GHz; and the operating bandwidth reaches 1.25 GHz.

Figure 8 shows the radiation direction of the planar array antenna. The data in the figure indicates that the peak gain of the antenna E-plane is 17.6 dBi, the side lobe level -21.1 dB, the peak gain of the antenna H-plane 17.6 dBi, the side lobe level -24.5 dB.

3.3. Array MIMO Antenna Design

In order to make the designed array antenna have the function of transceiver integration, the array antennas designed in the previous section are combined into a four-port array MIMO antenna. The structure of the antenna after further simulation optimization by CST is shown in Fig. 9. Table 1 shows the final dimensions of the antenna obtained after simulation and optimization.

4. SIMULATED AND MEASURED RESULTS ANALYSIS

In order to verify the performance of the antenna, the array MIMO antenna designed in the previous section is examined for planar case and bending case, respectively.

4.1. Planar Free Space

The proposed antenna array is simulated in CST Microwave Studio software, and the simulated results are compared and

FIGURE 5. Y-shape power divider structure.
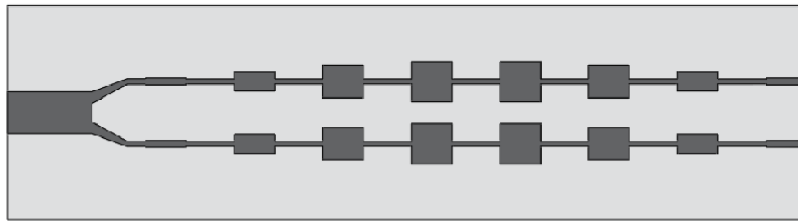
FIGURE 6. Structure of series-parallel hybrid fed planar antenna array.
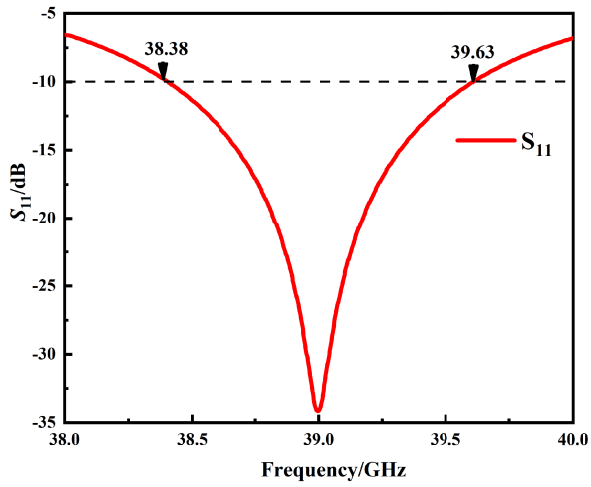
FIGURE 7. S-parameters of planar array antenna.
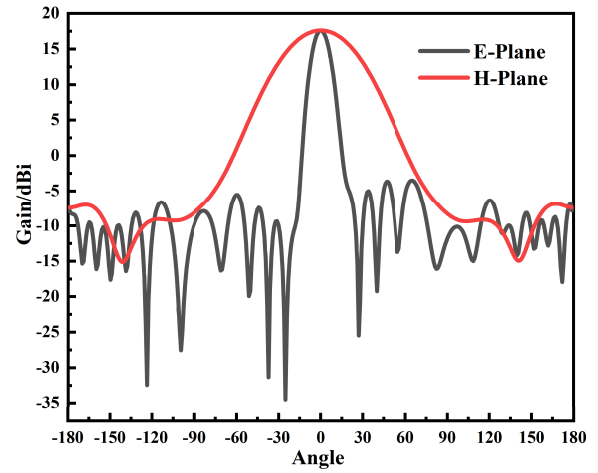
FIGURE 8. Planar array antenna radiation direction diagram.
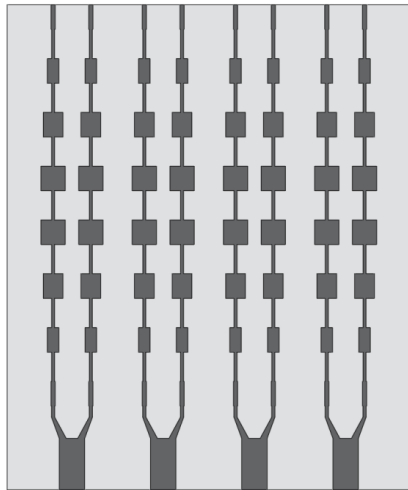
FIGURE 9. Final array antenna structure diagram.
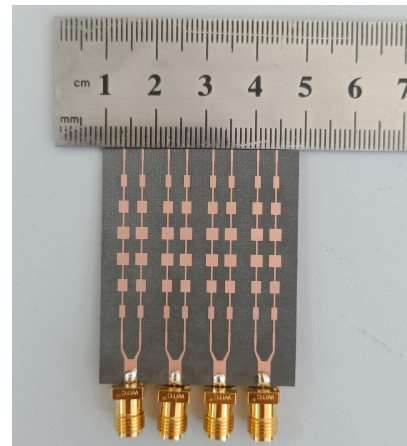
FIGURE 10. Antenna physical diagram.

TABLE 1. Geometric dimension of the antenna (mm).

parameter	value/mm	parameter	value/mm	parameter	value/mm
W_{P1}	0.413	L_i	2.869	W_i	0.297
W_{P2}	1.138	W_{100}	0.689	L	2.088
W_{P3}	1.948	W_f	2.511	L_P	2.425
W_{P4}	2.400	h	0.787	L	39.80
L_f	5.062	W	47.47	L_f	5.062

FIGURE 11. Antenna testing diagram.
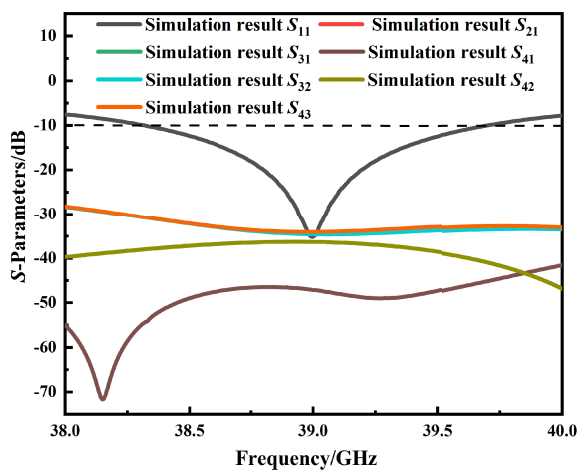
FIGURE 12. Simulated parameters.
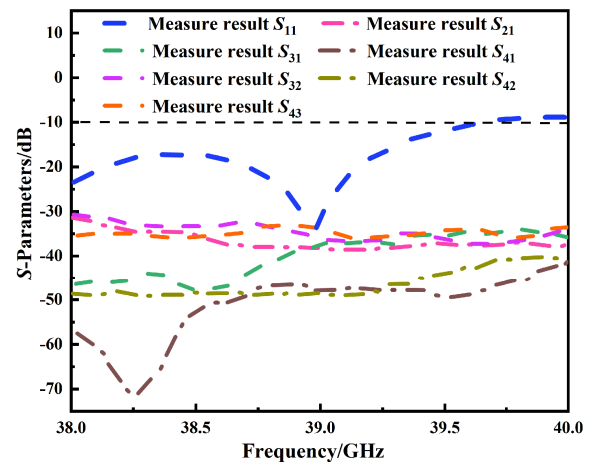
FIGURE 13. Measured parameters.

analyzed with the measured results. Fig. 10 is a photo of the physical antenna, and Fig. 11 is a photo of the antenna during S-parameter testing.

4.1.1. S-Parameters

Figure 12 and Figure 13 show the plots of simulated and measured results of the S-parameters of the array MIMO antenna, respectively. The data in the figures indicates that simulated and measured resonant frequencies of the antenna are both at 39 GHz; the simulated operating band is $38.32 \sim 39.73$ GHz; the measured operating band is $38.0 \sim 39.6$ GHz. The antenna isolation of each port is lower than -25 dB in the simulated results, and the antenna isolation of each port is lower than -30 dB in the measured results, which are in line with the design requirements of MIMO antenna.

4.1.2. Radiation Characteristics

The radiation direction diagrams of the antenna are shown in Fig. 14, and the 3 dB lobe widths of the antenna E plane and H plane are $12.2°$ and $49.2°$, respectively. The simulated and measured side lobe levels are -22.5 dB and -21.9 dB for the H-plane, respectively, and the simulated and measured side lobe levels are -20.6 dB and -20.2 dB for the E-plane, respectively. The results show that the antenna has consistency in the

radiation direction diagrams of the measured and simulated antennas.

4.1.3. Gain and Efficiency

The measured and simulated gains and efficiencies of the antenna are shown in Fig. 15. The data in the figure indicates that the antenna gain reaches its maximum near 39 GHz, at which time the simulated gain reaches 17.7 dBi, and the measured gain reaches 17.45 dBi. The measured results show that the antenna's gain is higher than 16 dBi in the entire working frequency band and that the antenna has a high radiation efficiency, which stabilizes in the working frequency band at about 99%.

4.1.4. ECC and DG

ECC and DG are important parameters of a MIMO antenna, and there is an inverse relationship between ECC and DG. The smaller the ECC is, the larger the DG is, and the smaller the coupling is between the elements. As shown in Fig. 16, the simulated ECC values in the entire frequency band is less than 0.003, meeting the standard value less than 0.5, and the simulated DG values are close to the standard value of 10. The overall DG is greater than 9.98 in the operating frequency band, indicating that the reduction of antenna transmission power will not have
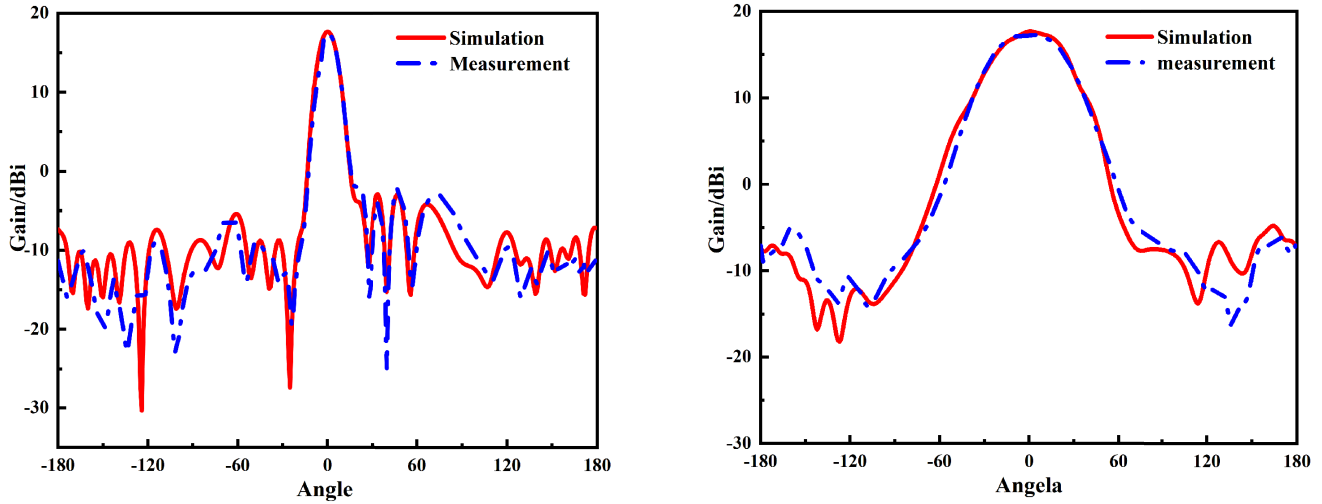
FIGURE 14. Radiation direction diagrams.
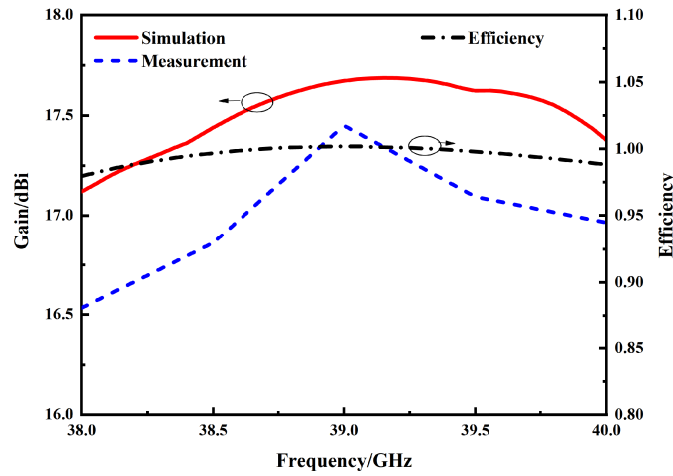
FIGURE 15. Gain and efficiency.
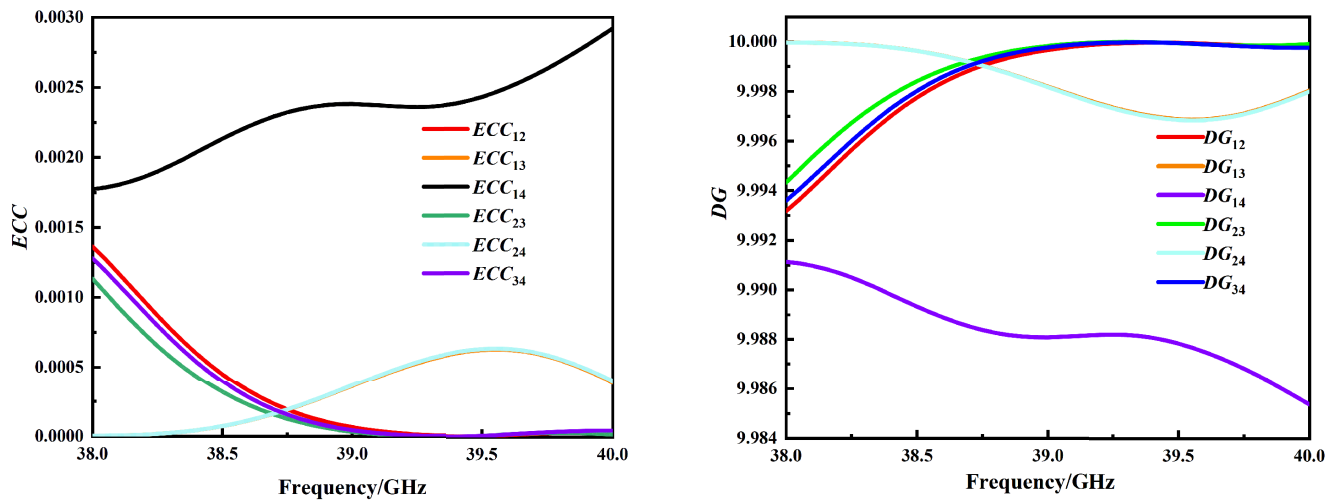
FIGURE 16. ECC and DG of the array MIMO antenna.
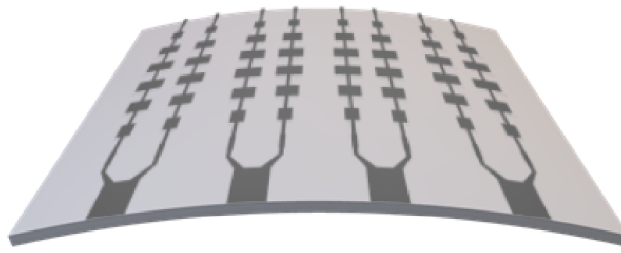
FIGURE 17. Schematic structural diagram of antenna bending.
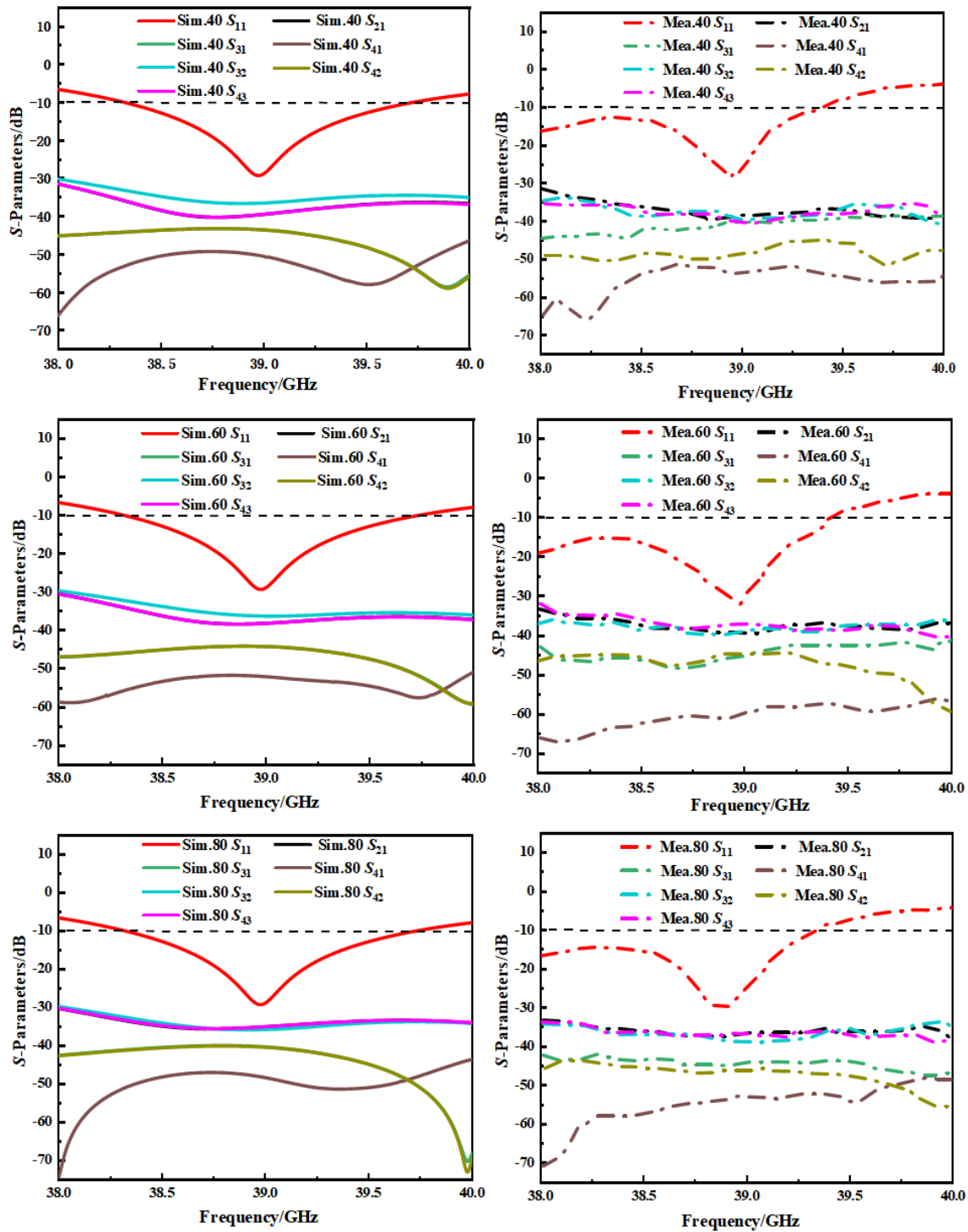
FIGURE 18. Simulated and measured S-parameters of antenna bending along different radii.
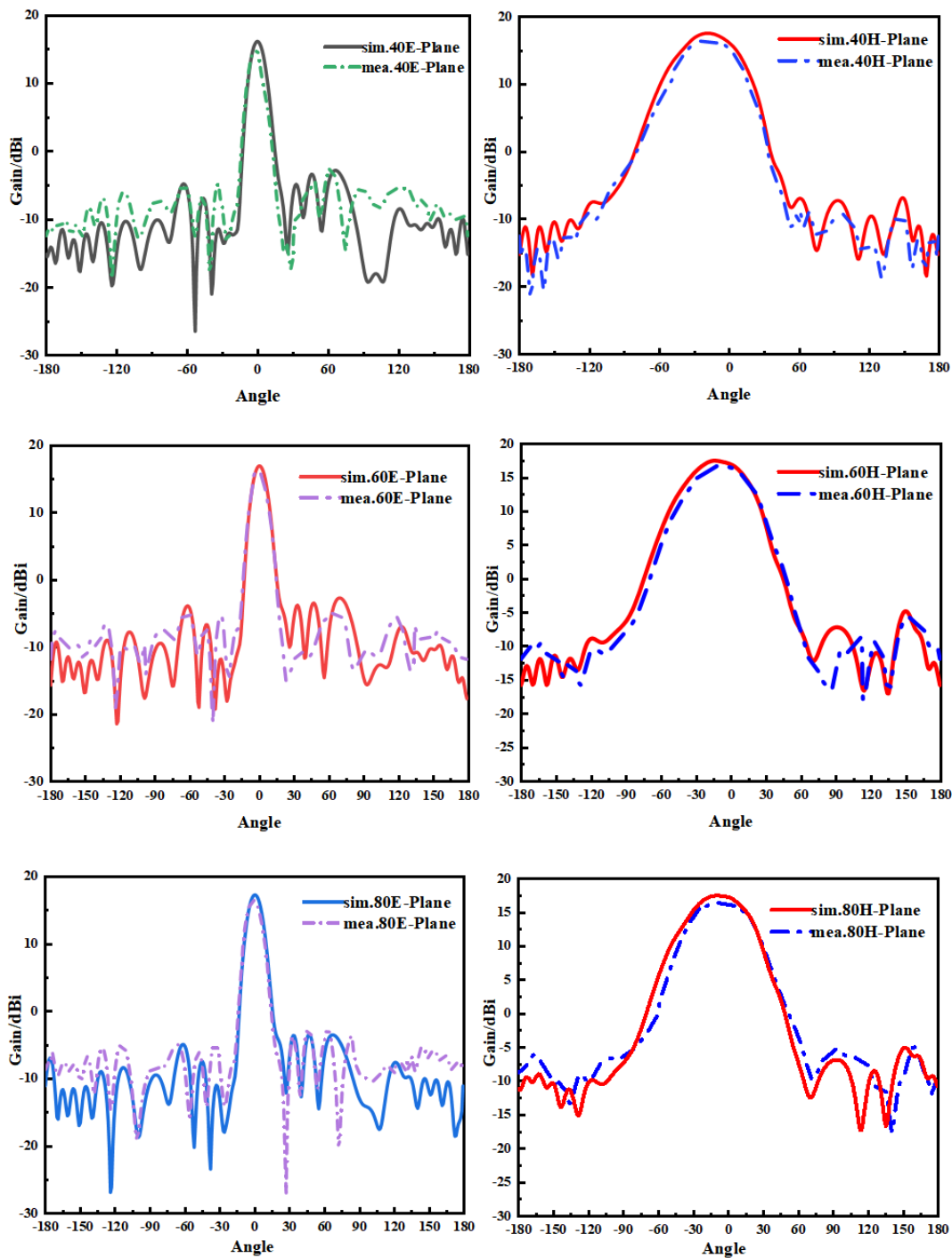
FIGURE 19. Antenna bending direction diagram along different radii.

much impact on MIMO transmission quality or performance. The simulated results show that the designed antenna elements have high independence from each other.

4.2. Bending Free Space

In a coupler online monitoring equipment, the applied antenna needs to have a certain bending radian and wear resistance, and flexible antennas have poor wear resistance. Rogers RT5880 has good wear resistance and is able to bend to a certain ex-

tent. Moreover, it will reduce its physical size while maintaining relatively stable antenna performance, which is especially important for space-limited occasions. In order to analyze the effect of antenna curvature on antenna performance, the four-port array MIMO antenna designed in the previous section is bent around the x-axis tightly against a cylinder with radius R. The antenna is then bent around the x-axis. When the microstrip antenna is bent, its characteristics are changed compared to the planar structure, and the degree of change is related to the curvature of the carrier. The change in size after bend-

TABLE 2. Comparison of the proposed antenna with previously reported antenna.

Ref.	Freq./GHz	ports	Iso./dB	gain/dBi	efficiency	SLL/dB	ECC	DG
[17]	28	4	< -30	6.5	—	—	0.18	—
[18]	28/38	2	< -20	8	80%	-10	0.0001	9.99
[19]	28	4	< -17	8.3	—	—	0.01	9.96
[20]	28	4	< -29	6.1	92%	—	0.16	—
[22]	28	2	< -28	15.46	93%	—	0.0001	—
[23]	37	2	< -40	12.8	85%	-11.7	0.00014	9.99
[24]	28	4	< -30	12.5	91.5%	$-5.6/-21.5$	0.00009	≈ 10
This work	39	4	< -30	17.45	99%	< -20	0.003	9.98
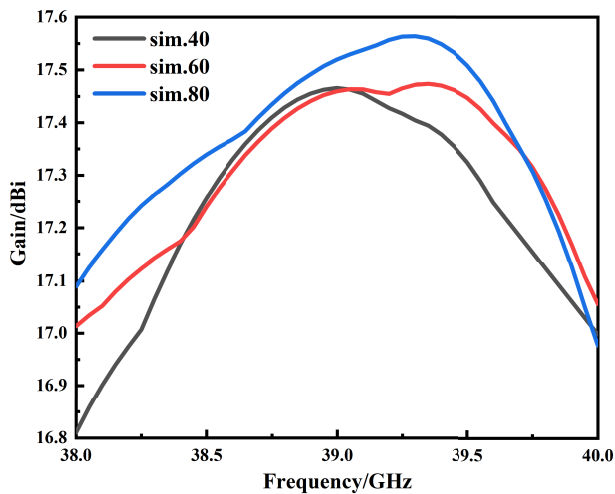
FIGURE 20. Antenna gain simulation diagram.

ing will change the current distribution on the patch, causing a shift in the resonant frequency. Therefore, the performance of the antenna has to be verified by simulation tests at different degrees of bending. The antenna bending schematic is shown in Fig. 17.

The S-parameters, radiation direction maps, and gains of the antenna are simulated for three bending degrees selected respectively and compared with the measured results.

As shown in Fig. 18, the resonant frequency of the antenna under different bending cases undergoes a slight shift. However, the -10 dB relative bandwidth (3.60%, 3.56%, and 3.47% for carrier radius R of 40, 60, and 80, respectively) does not change much, indicating that the antenna is well matched under different bending conditions and is able to work in normal operation.

Figure 19 shows the radiation direction diagram of the antenna, and it is found by comparison that when the array antenna is not bent, the maximum radiation direction of the main lobe of its E-plane and H-plane is at 0°; the gain reaches the maximum, and the maximum gain of the antenna decreases with the increase of the bending radian. In addition, as the antenna is bent, the feed port deviates from the originally defined z-axis direction, resulting in the radiation main lobe of the antenna deviating from 0°.

Figure 20 shows the simulated gain of the antenna under different degrees of bending. The data in the figure indicates that a larger bending will lead to a decrease in the antenna gain; the antenna gain drop is most pronounced when $R = 40$ mm; and the maximum antenna gain is 17.47 dBi. The gain is 0.23 dBi lower than that when the antenna is unbent.

Table 2 shows the performance comparison of the high gain MIMO array antenna proposed in this paper with the published array MIMO antennas. The comparative analysis shows that the antenna designed in this paper exhibits superior performance in a number of key performance metrics such as isolation, efficiency, and gain. As a result, the applicability of the proposed MIMO antenna in 5G millimeter-wave communication applications is established.

5. CONCLUSION

In this paper, a series-parallel hybrid-fed high-gain millimeter-wave array MIMO antenna is designed with the antenna dimensions of $47.47 \times 39.80 \times 0.787$ mm^3, and the antenna operates in the frequency band from 38.0 to 39.6 GHz. The series-parallel hybrid feeding technique is used to achieve a gain of 17.45 dBi at 39 GHz, and the side lobe levels of the antenna on E-plane and H-plane are -20.2 dB and -21.9 dB, respectively, by the Chebyshev synthesis method. In the operating frequency band, the antenna gain is higher than 16 dBi; the efficiency reaches 99%; the ECC is lower than 0.003; and the DG is greater than 9.98, which has satisfactory MIMO performance index. Secondly, the frequency and radiation characteristics of the antenna are analyzed in the case of column bending, and the results show that the resonant frequency is slightly shifted due to the bending of the antenna column, but the relative bandwidth is basically unchanged, and the antenna's gain decreases with the increase of bending radian, which still satisfies the working requirements of the current wireless communication system.

ACKNOWLEDGEMENT

REFERENCES

[1] Rappaport, T. S., Y. Xing, G. R. MacCartney, A. F. Molisch, E. Mellios, and J. Zhang, "Overview of millimeter wave communications for fifth-generation (5G) wireless networks — With a focus on propagation models," *IEEE Transactions on Antennas and Propagation*, Vol. 65, No. 12, 6213–6230, Dec. 2017.

[2] Khalily, M., R. Tafazolli, P. Xiao, and A. A. Kishk, "Broadband mm-Wave microstrip array antenna with improved radiation characteristics for different 5G applications," *IEEE Transactions on Antennas and Propagation*, Vol. 66, No. 9, 4641–4647, 2018.

[3] Mandloi, M. S., P. Gupta, A. Parmar, P. Malviya, and L. Malviya, "Beamforming MIMO array antenna for 5G-millimeter-wave application," *Wireless Personal Communications*, Vol. 129, No. 1, 153–172, 2023.

[4] Dzagbletey, P. A. and Y.-B. Jung, "Stacked microstrip linear array for millimeter-wave 5G baseband communication," *IEEE Antennas and Wireless Propagation Letters*, Vol. 17, No. 5, 780–783, 2018.

[5] Zhou, J., "Research and design of 77 GHz millimeter wave radar antenna array," University of Electronic Science and Technology, 2024.

[6] Hu, W., Q. Li, H. Wu, Z. Chen, L. Wen, W. Jiang, and S. Gao, "Dual-band antenna pair with high isolation using multiple orthogonal modes for 5G smartphones," *IEEE Transactions on Antennas and Propagation*, Vol. 71, No. 2, 1949–1954, 2023.

[7] Khalid, M., S. I. Naqvi, N. Hussain, M. Rahman, Fawad, S. S. Mirjavadi, M. J. Khan, and Y. Amin, "4-port MIMO antenna with defected ground structure for 5G millimeter wave applications," *Electronics*, Vol. 9, No. 1, 71, 2020.

[8] Wei, F., X. Liu, X.-Z. Ding, X.-B. Zhao, and P.-Y. Qin, "A balanced filtering antenna array with high gain, steep selectivity, and multi-radiation nulls parallel-fed by differential broadband network," *IEEE Transactions on Antennas and Propagation*, Vol. 71, No. 12, 9926–9931, Dec. 2023.

[9] Huang, D., G. Xu, J. Wu, W. Wang, L. Yang, Z.-X. Huang, X.-L. Wu, and W.-Y. Yin, "A microstrip dual-split-ring antenna array for 5G millimeter-wave dual-band applications," *IEEE Antennas and Wireless Propagation Letters*, Vol. 21, No. 10, 2025–2029, 2022.

[10] Ding, X. and Z. Chen, "An asymmetric millimeter wave MIMO antenna array for 5G applications," in *2023 IEEE 6th International Conference on Electronic Information and Communication Technology (ICEICT)*, 313–316, Qingdao, China, Sep. 2023.

[11] Geschke, R. H., C. S. Chaves, and C. Krebs, "Surface wave mitigation based on finite EBG structures for W-band radar millimetre-wave MIMO antenna arrays," in *2023 53rd European Microwave Conference (EuMC)*, 661–664, Berlin, Germany, Oct. 2023.

[12] Chithradevi, R. and B. S. Sreeja, "A compat UWB MIMO antenna with high isolation and low correlation for wireless applications," in *2017 IEEE International Conference on Antenna Innovations & Modern Technologies for Ground, Aircraft and Satellite Applications (iAIM)*, 1–4, Bangalore, India, 2017.

[13] Rajkumar, S., A. A. Amala, and K. T. Selvan, "Isolation improvement of UWB MIMO antenna utilising molecule fractal structure," *Electronics Letters*, Vol. 55, No. 10, 576–579, 2019.

[14] Manage, P. S., U. Naik, S. Kareemulla, and V. Rayar, "Dual band notched UWB-MIMO antenna incorporating CSRR for WLAN and X band applications," in *2020 Third International Conference on Smart Systems and Inventive Technology (ICSSIT)*, 149–152, Tirunelveli, India, 2020.

[15] Shen, X., Y. Liu, L. Zhao, G.-L. Huang, X. Shi, and Q. Huang, "A miniaturized microstrip antenna array at 5G millimeter-wave band," *IEEE Antennas and Wireless Propagation Letters*, Vol. 18, No. 8, 1671–1675, 2019.

[16] Zhou, X., H. Zhai, L. Xi, Z. Wei, S. Ma, and L. Zheng, "A low-profile four-element MIMO antenna array with new decoupling structures," *Microwave and Optical Technology Letters*, Vol. 60, No. 10, 2511–2516, 2018.

[17] Shariff, B. G. P., A. A. Naik, T. Ali, P. R. Mane, R. M. David, S. Pathan, and J. Anguera, "High-isolation wide-band four-element MIMO antenna covering Ka-band for 5G wireless applications," *IEEE Access*, Vol. 11, 123 030–123 046, Oct. 2023.

[18] Tsao, Y.-F., A. Desai, and H.-T. Hsu, "Dual-band and dual-polarization CPW fed MIMO antenna for fifth-generation mobile communications technology at 28 and 38 GHz," *IEEE Access*, Vol. 10, 46 853–46 863, 2022.

[19] Khalid, M., S. I. Naqvi, N. Hussain, M. Rahman, Fawad, S. S. Mirjavadi, M. J. Khan, and Y. Amin, "4-port MIMO antenna with defected ground structure for 5G millimeter wave applications," *Electronics*, Vol. 9, No. 1, 71, 2020.

[20] Kamal, M. M., S. Yang, X.-c. Ren, A. Altaf, S. H. Kiani, M. R. Anjum, A. Iqbal, M. Asif, and S. I. Saeed, "Infinity shell shaped MIMO antenna array for mm-Wave 5G applications," *Electronics*, Vol. 10, No. 2, 165, 2021.

[21] Tariq, S., S. I. Naqvi, N. Hussain, and Y. Amin, "A metasurface-based MIMO antenna for 5G millimeter-wave applications," *IEEE Access*, Vol. 9, 51 805–51 817, Mar. 2021.

[22] Mandloi, M. S., P. Gupta, A. Parmar, P. Malviya, and L. Malviya, "Beamforming MIMO array antenna for 5G-millimeter-wave application," *Wireless Personal Communications*, Vol. 129, No. 1, 153–172, 2023.

[23] Khan, J., S. Ullah, U. Ali, F. A. Tahir, I. Peter, and L. Matekovits, "Design of a millimeter-wave MIMO antenna array for 5G communication terminals," *Sensors*, Vol. 22, No. 7, 2768, 2022.

[24] Sehrai, D. A., M. E. Munir, S. H. Kiani, N. Shoaib, A. D. Algarni, H. Elmannai, M. M. Nasralla, and T. Ali, "A high gain array based millimeter wave MIMO antenna with improved isolation and decorrelated fields," *IEEE Access*, Vol. 12, 89 794–89 803, 2024.

[25] Dash, J. C., D. Sarkar, and Y. M. M. Antar, "Design of series-fed antenna array with low sidelobe level and improved azimuth fied-of-view for automotive RADAR application," in *2023 XXXVth General Assembly and Scientific Symposium of the International Union of Radio Science (URSI GASS)*, 1–4, Sapporo, Japan, 2023.

[26] Fang, C., M. Su, and Y. Liu, "A low side lobe level microstrip antenna array for 77 GHz automotive radar," in *2020 IEEE 6th International Conference on Computer and Communications (ICCC)*, 448–452, Chengdu, China, 2020.

[27] Li, B., Y. Qiu, J. Zhang, Y. Deng, Z. Zhou, and L. Sun, "W-band high-gain hybrid-fed microstrip patch array with low sidelobe patterns," in *2020 International Conference on Microwave and Millimeter Wave Technology (ICMMT)*, 1–3, Shanghai, China, 2020.

[28] Wei, W. and X. Wang, "A 77 GHz series fed weighted antenna arrays with suppressed sidelobes in *E*- and *H*-plane," *Progress In Electromagnetics Research Letters*, Vol. 72, 23–28, 2017.

[29] Ram, N., H. Gao, M. S. Sadiq, and A. C. Bahadur, "77 GHz corporate feed series microstrip antenna array for the applications of automotive radar," in *2020 9th Asia-Pacific Conference on Antennas and Propagation (APCAP)*, 1–2, Xiamen, China, 2020.